Third International Conference on Biaxial/Multiaxial Fatigue
April 3-6, 1989, Stuttgart, Federal Republic of Germany

EXTENSION OF OVERSTRESS CONCEPT FOR BIAXIAL CREEP-FATIGUE BEHAVIOR

Toshiya Nakamura, Tomonari Ishikawa and Yasuhide Asada
Department of Mechanical Engineering, The University of Tokyo
Bunkyo-ku, Tokyo 113 Japan

1. Introduction

The creep-fatigue life prediction is one of major concerns in a structural design of high temperature components in order to assess their structural integrity. In the authors' previous studies with 304 stainless steel[1-5], push-pull strain control creep-fatigue tests have been conducted at 650°C in a very high vacuum of 0.1 μPa. The result suggested that even in this high vacuum environment the steel showed a time dependent reduction of a fatigue life. The test environment was almost free from the effect of air environment. The authors called the observation as the "pure" creep-fatigue behavior. In this environmental effect free condition, the frequency effect diminished and a creep-fatigue life showed an increase by about one order of magnitude from that in air. However, a time-dependent life reduction still remained and was affected from a strain wave shape.

Under a uniaxial push-pull loading in an environmental effect free condition, a time-dependent life reduction occurs when a time for a tension going stroke is larger than a time for compression going one. In case that the former is equal to or less than the latter, no life reduction was observed. This trend was concluded from a wide variety of a strain wave shape of a symmetric continuous cycle, an unsymmetric continuous cycle and a hold-time cycle, with a strain rate of 10**-5 to 10**-3 1/s and a hold-time up to 600 s.

The overstress concept[6] was applied for explaining the observation and the sucessful result was attained for treating the "pure" creep-fatigue life prediction.

It is the purpose of the present study to extend an applicability of this overstress concept to a biaxial creep-fatigue life prediction of 304 stainless steel at 650°C in air.

2. Overstress Concept for Creep-Fatigue Evaluation

The overstress is defined as a difference between an externally applied stress and an internal back stress and is assumed to be the primary driving force for a development of an inelastic deformation. The inelastic deformation occurs in a direction of the overstress and ceases when the overstress is equal to zero.

As to an experimental side, a particular bowing-out shape is usually observed in an unloading part of a stress-strain hysteresis curve obtained in creep-fatigue tests. An inelastic strain develops in a direction of a working stress at the moment just after unloading starting. This development of the inelastic strain decreases in its rate to take an extreme and then the development occurs in an opposit direction to the previous one. This behavior becomes dominant as a decrease of the unloading strain rate.

The overstress concept suggests that an externally applied stress coincides with the back stress at the moment when the inelastic strain takes an extremity. This means that a value of the back stress at the moment can be determined experimentally through computing a value of a stress corresponding to this extreme in the inelastic strain. The procedure is equivalent to the stress dip technique[7] developed to determine an internal stress during creep.

An observed overstress was defined by a difference between a peak value of a stress at strain reversal and thus determined back stress and was examined with respect to its dependency on the unloading strain rate. The observed overstress showed a decrease as an increase of the unloading strain rate and a saturation at about 10**-3 1/s unloading strain rate. This trend means a time dependent recovery of the back stress during unloading and the recovery can be neglected at a higher unloading strain rate exceeding 10**-3 1/s. This saturated value of the observed overstress can be considered a value of the overstress working at a moment just prior to unloading starting.

In order to establish a constitutive relation between the overstress and the inelastic strain rate, a value of the overstress was correlated with an inelastic strain rate just prior to unloading starting. In case of 304 steel, the relation shows an increase of the overstress as an increase of the inelastic strain rate which is lower than 5 x 10**-5 1/s. At higher strain rate region, the overstress is not sensitive to the inelastic strain rate. This suggests that the inelastic deformation is rate sensitive at lower strain rate less than 5 x 10**-5 1/s but is rate insensitive at higher strain rate. The former means a creep deformation and the latter plasticity.

By using this overstress-inelastic strain rate relation, a stress-strain response was analyzed to determine a value of the overstress at an arbitrary moment of loading and following damage modeling was examined based on overstress.

A time-independent damage parameter D_I and a time-dependent damage parameter D_D were defined by following eqs.(1) to (3).

$$D_I = \int_{cycle} \sigma_e d\varepsilon_p \quad (1)$$

$$D_D = \int_{cycle} \sigma_e dt \quad (2)$$

$$D_D = 0 \quad ; \text{ if eq.(2) gives a negative value} \quad (3)$$

where, σ_e is an overstress, ε_p is an inelastic strain and t is a time. The creep-fatigue life fraction was correlated with D_I and D_D through eqs.(4) and (5), where N_{f0} and N_f are the fatigue life and the creep-fatigue life, respectively. By using material parameters C_1, C_2, α_1 and α_2,

$$\Phi_I = 1/N_{f0} = C_1 D_I^{**}\alpha_1 \quad (4)$$

$$\Phi_D = 1/N_f - 1/N_{f0} = C_2 D_D^{**}\alpha_2 \quad (5)$$

The life evaluation equation is given by a linear summation of the time-independent damage Φ_I and the time-dependent damage Φ_D as following.

$$\Phi_I + \Phi_D = 1 \quad (6)$$

3. Biaxial Creep-Fatigue Tests

A solution annealed 304 stainless steel was tested by using a thin walled tublar specimen which has an inner diameter of 12 mm, wall thickness of 2 mm and gage length of 30 mm. The chemical composition of the test material is given in Table 1. The specimen has circumferencial ridges at both ends of the gage length for mounting the biaxial extensometer. Flanges were welded at both ends of the specimen to connect it to the testing machine.

A biaxial tension-torsion creep-fatigue testing machine was employed. The system is driven with an electro-hydraulic closed loop system using a linear actuator and a rotary actuator. A specimen is heated with an infra-red heating furnace to obtain a uniform thermal distribution along a specimen axis.

A biaxial extensometer employed uses a phto sensor for an axial displacement and aRVDT for arotation displacement. Axial and rotational displacements at gage sections are led with two sets of straight bars out of the furnace. A ring is connected to the other end of each set of bars. Two rings are arranged coaaxially to the loading axias by using ball-roller supporting devices. The relative motion of the rings are measured with above mentioned sensors.

Biaxial creep-fatigue tests were conducted at 650°C in air under a proportional total strain condition. A strain wave shape includes a symmetric continuous, unsymmetric continuous and hold-time cycle with a strain rate of 10**-5 to 10**-3 1/s and a hold-time of 600 s. A value of a proportional ratio λ ranges from 0 (pure axial) to (pure shear), where λ is defined by eq.(7).

$$\lambda = \gamma/\varepsilon\sqrt{3} \quad (7)$$

where, ε is the axial total strain and γ is the total engineering shear strain. A test condition was determined based on an eqivalent total strain ε_{eq}

given by eq.(8). An equivalent stress σ_{eq} is defined by eq.(9).

$$\varepsilon_{eq} = (\varepsilon^{**}2 + \gamma^{**}2/3)^{**}0.5\,\mathrm{sgn}(\varepsilon + \gamma/\sqrt{3}) \quad (8)$$

$$\sigma_{eq} = (\sigma^{**}2 + 3\tau^{**}2)^{**}0.5\,\mathrm{sgn}(\sigma + \tau\sqrt{3}) \quad (9)$$

Table 2 summarizes a condition of the present biaxial creep-fatigue tests.

For further analyses of data on stress-strain responses, on-line data acquisition was accomplished with a personal computer OKI if-800 Model 60 with an appropriate sampling time interval of 10 ms to 100 ms. The sampled data were transfered to a mini-computer OKITAC System 50V for further analyses.

4. Results of Biaxial Creep-Fatigue Tests

Figure 1 summarizes a relation between an equivalent total strain range and a fatigue life of the present tests. Lines in the figure indicate a trend of strain range versus fatigue life relations obtained under uniaxial loading in air and vacuum with a symmetric continuous cycle of a strain rate of 10**-3 1/s.

A following trend can be seen from the figure although there exists some ambiguity due to a limited number of biaxial data points. In case of the pure shear cycle, a symmetric continuous cycle of 10**-3/10**-3 1/s and 10**-4/10**-4 1/s and an unsymmetric cyle of 10**-4/10**-3 1/s show almost same fatigue life which is almost coincides with that of uniaxial cycling in air at a strain range of 0.01. A small increase of a fatigue life is observed at a strain range of 0.006 under biaxial condition compared with a unixaial condition. Other data points show a reduction of a fatigue life in biaxial loading from that in uniaxial cases.

A gradient of the strain range versus life relation of biaxial data is not steeper than that of uniaxial data in air but is almost parallel to a line indicating the uniaxial data in vacuum. Except for a shorter fatigue life in biaxial data in air than uniaxial data in vacuum, these two kinds of fatigue data have a similar trend with respect to a time-rate dependent behavior of the strain range versus life relation.

A macroscopic failure mode of the present biaxial test specimens shows an X-type crack development, as well known. A crack initiates at first perpendicular or parallel to a specimen axis and then it propagates into an oblique direction to the axis to form the X-type failure mode. The macroscopic crack propagates into a direction perpendicular to the maximum principal stress in case of a symmetric strain wave shape. A longer macroscopic crack is observed in a direction perpendicular to the principal stress which for a longer duration, in case of unsymmetric cycles.

5. Stress-Strain Response and Analysis of Overstress

The present material shows a typical cyclic strain hardening behavior as shown in Fig. 2 which gives an example observed through a symmetric continuous

cycle with a strain rate of 10**-3 1/s and a strain range of 0.01 under a proportional ratio of $\lambda = 1$. The cyclic strain hardening almost saturates by a number of strain cycles of about 10 per cent of the fatigue life. The hardening behavior is almost similar with respect to the axial stress, the shear stress and the equivalent stress.

Figure 3 summarizes the cyclic strain hardening behavior of the eqivalent stress obtained under an equivalent total strain range of 0.01, equivalent total strain rate of 10**-3 1/s and a proportional ratio of 0 to ∞. The data plots show a reasonable coincidence regardless the difference of the proportional ratio. In addition, the trend coincides with the cyclic strain hardening behavior observed by uniaxial tests in air and vacuum. The stress-strain response is not affected by a test environment as already checked in the previous uniaxial tests.

Figure 4 gives an example of the stress loci of the axial stress versus shear stress obtained in the present biaxial tests. These three figures show a following common trend. At the peaks of strain reversals, the stress locus coincides with a locus of the total strains. During unloading from the stress peaks, a faster unloading rate is seen in a shear component of a stress than an axial stress component so that the stress locus leaves from the strain locus. Then a stress locus changes its direction to become parallel to the strain locus. Finally, the stress locus changes its direction toward the strain locus to approach the strain locus. The first stage corresponds to the unloading from a stress peak to a back stress. Second one corresponds to a quasi-elastic reloading process and third one corresponds a development of major inelastic deformation. In the figures, symbols indicate the points of the back stress determined through a procedure mentioned later.

As to the overstress and the back stress, the unloading curve of stress-strain hysteresis loops was analyzed by using a same procedure employed in the previous study on uniaxial creep-fatigue tests. In the present study, the analysis was made with respect to component stress-strain relations and an equivalent stress-strain relation, respectively. The values of a back stress were determined by fitting a quadratic curve to the unloading stress-strain relation to find an extreme of the inelastic strain as examplly shown in Fig.5.

In Table 3, the result of the analysis is summarized. σ_e and τ_e are the axial and shear component of the overstress, respectively. σ_b and τ_b are the axial and shear component of the back stress, respectively. A small difference is observed between the values determined from component stress-strain relations and those from the equivalent stress-strain relation. The circles in Fig. 4 shows a back stress determined from the equivalent relation. The triangle was obtained from component stress-strain relations.

The time-dependent recovery of the observed overstress or the back stress was examined again with the result of the analysis of the present biaxial study. Figure 6 shows a relation between the observed value of the overstress and the unloading strain rate. The value of the overstress is given by an equivalent value and the unloading strain rate, too. In the figure, data points are also plotted which were obtained in the previous uniaxial tests.

It can be concluded that the observed overstress shows almost saturation at an unloading strain rate of 10**-3 1/s as it was in the uniaxial study, although the figure shows a wider scatter of the data. As previously mentioned, this recovery of the observed overstress caused from a relaxation of the back stress during unloading. As a result, the authors considered that a correct value of the overstress at a stress peak is given by a saturated value of the observed overstress at an unloading strain rate of 10**-3 1/s, as it was considered in the previous uniaxial study.

Figure 7 shows a loading strain rate dependency of the overstress at strain reversals, that is a relation between an inelastic strain rate just prior to unloading starting and the overstress at this moment. The figure also includes data points from present biaxial tests and previous uniaxial tests in a form of equivalent stress and equivalent strain rate.

A wide scatter is also seen in the figure, however, a trend of data indicates that almost constant overstress is seen with respect to the inelastic strain rate, in case of pure shear loading. The authors cnsidered that the overstress versus inelastic strain rate relation may be affected from a resolved normal stress or a hydrostatic stress. If this estimation holds good, the overstress under pure shear loading is held constant with respect to the loading inelastic strain rate. This estimation leads us to information that a shear component of the overstress controls a time-independent inelastic deformation and that the time-dependent inelastic deformation is caused under an effect of a resolved normal or hydrostatic component of the overstress.

In Fig. 8, a summary of the observations is given with respect to a mechanical response of peak stresses and back stresses, in a $\sigma - \tau\sqrt{3}$ biaxial stress plane. As already described, the stress components at peaks are well arranged by the Von Mises equivalent stress given by eq.(9) as easily seen in Fig.8. Values of the back stress components are given in the figure by those determined based on the equivalent stress-strain relation in Table 3. As shwon in the figure, data plots of the back stress components show some deviation from the Von Mises criterion. A major deviation is seen in a shear component of the back stress. This trend corresponds to the previous observation that the unlaoding rate of a shear stress component was faster than that of an axial stress.

Finally in Fig.9, a behavior of stress components is shown during a long

term stress relaxation for 20 hrs. which was introduced after 100 strain cycles by a symmetric continuous cycle with a strain range of 0.01 and a strain rate of 10**-3 1/s under proportional loading. The locus shows the axial versus shear stress relation during strain hold-time. In the figure, plots are given for indicating a state of the back stress components obtained from other specimen tested under a symmetric continuous cycle of the same condition. One plot indicates the back stress state obtained based on the equivalent stress-strain relation and the other on the component stress-strain relations. A trend is very clearly seen that a relaxation of stress components occurs at first in a direction toward the back stress and then changes its direction toward the total strain locus. The first stage of the relaxation means a relaxation of the overstress takes a main role. The second stage means a relaxation of the back stress. This is equivalent to the annealing process of the material. Of course, a small part of stress relaxation is taken by a contribution of the back stress in the first stage and by the overstress in the second stage. As to a time, the first stage was accomplished by about 5 hrs. of relaxation time. After then the second stage was observed.

6. Extension of Damage Modeling to Biaxial Straining

As already proposed in the modeling of biaxial/multiaxial fatigue, creep and creep-fatigue damages, the authors considered that stresses and strains are devided into a resolved shear component and a resolved normal component due to a difference between their contributions to the time-independent failure mode. In the present modeling, the authors devided the overstress into the resolved shear and normal components.

The authors dfined Π-plane which is a plane in a solid that gives a maximum shear component of the overstress. On the plane, following two components were defined in order to describe the time-independent component of the damage parameter D_I.

$$D_I^s = \int_{cycle} (\tau^p - \tau_b^p)\, d\gamma_p^p \qquad (10)$$

$$D_I^n = \int_{cycle} (\sigma^p - \sigma_b^p)\, d\varepsilon_p^p \qquad (11)$$

where, D_I^s and D_I^n are the components of the time-independent damage parameter D_I relating to the shear and normal component of the overstress, respectively. A superscript p means that the quantities are determined on the Π-plane. Other symbols mean as already explaned.

Based on the BSK Parameter[8], D_I is given by eq.(12) as following.

$$D_I = (D_I^{s}**j + D_I^{n}**j)**(1/j) \qquad (12)$$

A material constant j is determined through experiments and analyses of data.

Equations (10) and (11) are approximated by following eqs.(10') and (11') in order to be coordinated with the experiment, respectively.

$$D_I^s = \tau_{er}^p \gamma_{pr}^p \tag{10'}$$

$$D_I^n = \sigma_{er}^p \varepsilon_{pr}^p \tag{11'}$$

where, subscripts p and r means the inelastic component and the range, respectivel

The resolved shear and normal components of the overstress are computed by following eqs.(13) and (14), respectively, and the direction of the Π-plane is given by eq.(15).

$$\tau_e^p = -(1/2)\sigma_e \sin(2\theta) + \tau_e \cos(2\theta) \tag{13}$$

$$\sigma_e^p = \sigma_e (1 + \cos(2\theta))/2 + \tau_e \sin(2\theta) \tag{14}$$

$$\theta = \arctan(-\sigma_e/2\tau_e)/2 \tag{15}$$

A value of D_I given by eq.(12) is basically available to describe the "pure" creep-fatigue condition which is free from the environmental effect. Following extension was made in order to take into account the particular effect of the air environment which is superposing upon the "pure" creep-fatigue behavior in the present biaxial data, as those were obtained through tests in air.

$$D_I = (D_I^{s**j} + \Lambda(\dot{\varepsilon}_{eq}) D_I^{n**j})^{**(1/j)} \tag{16}$$

he function Λ represent the effect of air environment in terms of the strain rate $\dot{\varepsilon}_{eq}$ and is given by eq.(17) which was empirically derived based on the uniaxial cree-fatigue tests in air.

$$\Lambda(\dot{\varepsilon}_{eq}) = 2.37\text{x}10^{**(-3)} \dot{\varepsilon}_{eq}^{**(-0.75)} \tag{17}$$

And the value of j, the exponent in eq.(16) is given emprically as following.

$$j = 1.73 \tag{18}$$

As already stated, eq.(16) gives a value of D_I which takes into account the environmental effect of air. The D_I was correlated with a life fraction $1/N_{f0}$ of the present biaxial test data. Figure 10 shows the relation between the time-independent damage parameter and the time-independent life fraction to result in a following empirical relation.

$$\Phi_I = 1/N_{f0} = \exp(-7.29 D_I^{**(-0.154)}) \tag{19}$$

As to the time-dependent damage parameter, D_D was also extended to be applicable for the multiaxial stress state as eq.(20) which means a maximum value of the time integration of the principal stresses.

$$D_D = \max(\int_{cycle} \sigma_e^i dt) \quad ; \quad i = 1, 2 \text{ and } 3, \tag{20}$$

where, the superscript i means the index denoting the principal stresses. The expression by eq.(20) meets the definition of D_D in the uniaxial case. Based on an examination with respect to the uniaxial data in air and vacuum,

it was suggested that the value of D_D is not sensitive to the environmental effect. The authors considered that the expression by eq.(20) can be available to the present test data in air without further extension.

The D_D was correlated with the time-dependent life fraction of the present biaxial data in air. The result is shown in Fig. 11 and is empirically expressed by eq.(21).

$$\Phi_D = 1/N_f - 1/N_{f0} = 2.41\text{x}10^{**}(-7)D_D^{**}0.872 \qquad (21)$$

where, N_f is the fatigue life under a general strain wave shape.

As a result, following life prediction equation is given in a form of linear damage rule.

$$\Phi_I + \Phi_D = 1 \qquad (22)$$

Figure 12 shows a comparison between the experimental fatigue life and the predicted fatigue life given by eq.(22). In the figure, included are the uniaxial data in air, also. As seen in the figure, the present overstress concept gives a predicted life within a factor of 2.

7. Conclusion

An overstress concept was applied to the tension-torsion biaxial creep-fatigue behavior. The overstress and back stress were experimentally determined for the biaxial stress state and were correlated with the uniaxial stress state. A damage model was extended for biaxial creep-fatigue life evaluation, based on the overstress approach with a further extension for taking into account the environmental effect of air. A life prediction equation was empirically derived which gives a predicted life with a factor of two.

Acknowledgement

The authors express their harty thanks to Mr. A. Ishikawa of the University of Tokyo and Mr. S. Mitsuhashi of Shimazu Mfg. Ltd. for their collaboration in the experimental side of the present study. Thanks are also given to Mr. T. Meshii and Dr. H. Wada of Mitsubishi Heavy Industries for their helps to the study.

References

[1] Morishita, M. and Asada, Y., NED 83(1984)367-377

[2] Morishita, M., Taguchi, K., Satake, M. and Asada, Y., Proc. ICPVT-5 Part.II(1984)1109-1120

[3] Morishita M. and Asada, Y., Bull. JSME 28(1985)7-12

[4] Morishita, M., Taguchi, K., Asada, Y. etal, ASTM STP942(1987)487-499

[5] Asada, Y. etal, ASME Pub. PVP-129(1988)93-99

[6] Krempl, E., Jr. EMT 101(1979)380-386

[7] Ahlquist, C.N. and Nix, D., Scripts Metallurgica 3(1969)679-682

[8] Brown, M.W. and Miller, K.J., PIME 187(1973)

Table 1 Chemical Composition wt% (304 Stainless Steel 1120°C WC)

C	Si	Mn	P	S	Cu	Ni	Cr
0.07	0.56	1.60	0.023	0.007	0.04	9.40	18.3

Table 2 Loading Condition of Biaxial Tests

λ	ε_{eqr}	ε_{tr}	γ_{tr}	$\dot{\varepsilon}_{eq}$ (sec^{-1})	t h (sec)	NOTE
0	0.01	1.0	—	$10^{-3}/10^{-3}$	0	*
0	0.01	1.0	—	$10^{-3}/10^{-3}$	600	*
0.5	0.01	0.00894	0.00774	$10^{-3}/10^{-3}$	0	*
1	0.01	0.00707	0.0122	$10^{-3}/10^{-3}$	0	
2	0.01	0.00447	0.0155	$10^{-3}/10^{-3}$	0	
∞	0.01	—	0.0173	$10^{-3}/10^{-3}$	0	
∞	0.006	—	0.0104	$10^{-3}/10^{-3}$	0	
∞	0.01	—	0.0173	$10^{-4}/10^{-4}$	0	
∞	0.006	—	0.0104	$10^{-4}/10^{-4}$	0	
∞	0.01	—	0.0173	$10^{-4}/10^{-3}$	0	
∞	0.01	—	0.0173	$10^{-5}/10^{-3}$	0	
∞	0.01	—	0.0173	$10^{-3}/10^{-3}$	600	
1	0.01	0.00707	0.0122	$10^{-3}/10^{-3}$	—	**

*…Break at the Gage Point

**…Total Strain Hold at ε_{eq}=0.005 for 22hrs after 100 cycle

Table 3 Observed Values of the Overstress and Back Stress

	Component Base (MPa)						Equivalent Base (MPa)					
λ	σ_b	τ_b	σ_{beq}	σ_e	τ_e	σ_{eeq}	σ_b	τ_b	σ_{beq}	σ_e	τ_e	σ_{eeq}
0	178	0	178	74.0	0	74.0	178	0	178	74.0	0	74.0
	-215	0	-215	-37.0	0	-37.0	-215	0	-215	-37.0	0	-37.0
0.5	198	16.4	200	16.0	48.3	85.3	192	46.4	208	20.0	18.2	37.3
	-151	-23.8	-157	-35.3	-46.4	-88.2	-130	-36.2	-144	-56.0	-34.2	-81.6
1	130	45.3	152	30.4	58.8	107	122	63.5	164	39.0	40.4	80.1
	-118	-45.3	-142	-15.8	-62.8	-112	-101	-61.2	-146	-44.0	-81.0	-147
2	69.6	48.1	109	53.9	84.3	156	70.0	41.9	101	53.0	90.4	165
	-46.1	-65.8	-123	-45.1	-67.9	-126	-60.0	-46.9	-101	-18.0	69.3	-121
∞	0	98.2	170	0	43.0	74.5	0	98.2	170	0	43.0	74.5
	0	-81.4	-141	0	-48.1	-83.3	0	-81.4	-141	0	-48.1	-83.3
∞^*	0	98.1	170	0	35.2	61.0	0	98.1	170	0	35.2	61.0
	0	-76.2	-132	0	-56.1	-97.2	0	-76.2	-132	0	-56.1	-97.2
∞^{**}	0	51.9	90.0	0	57.8	100	0	51.9	90.0	0	57.8	100
	0	-67.4	-117	0	-78.6	-136	0	-67.4	-117	0	-78.6	-136

* $\dot{\varepsilon}_{eq} = 10^{-4}$ /10^{-3} (1/sec)

** 10^{-5} /10^{-3} (1/sec)

Upper Value ---- Tension (Forward Stroke)

Lower Value ---- Compression (Backward Stroke)

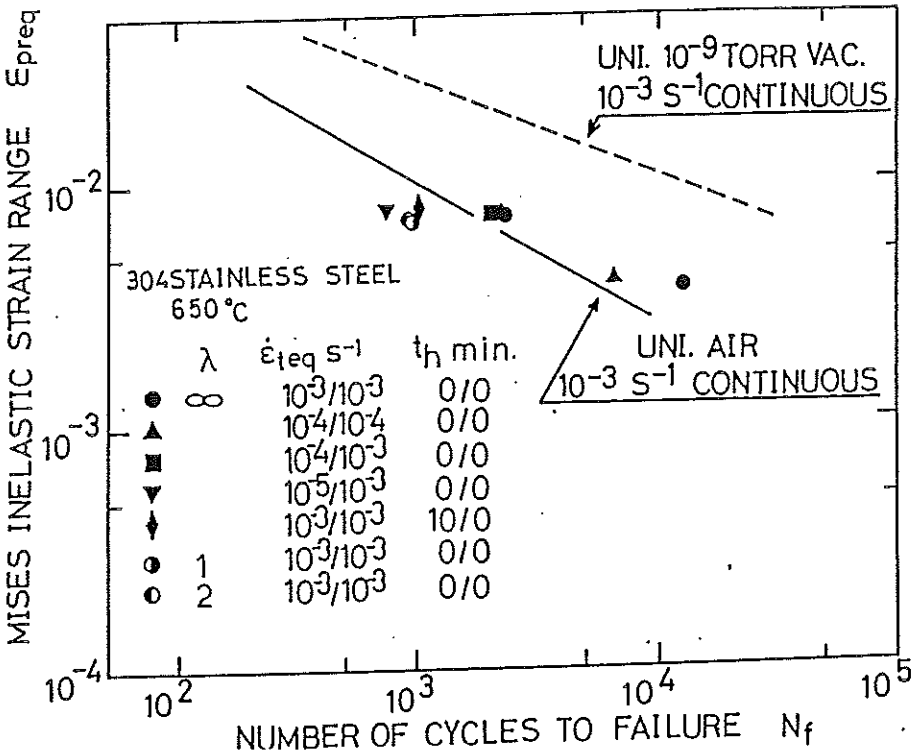

Fig. 1 Equivalent Inelastic Strain Range versus Fatigue life

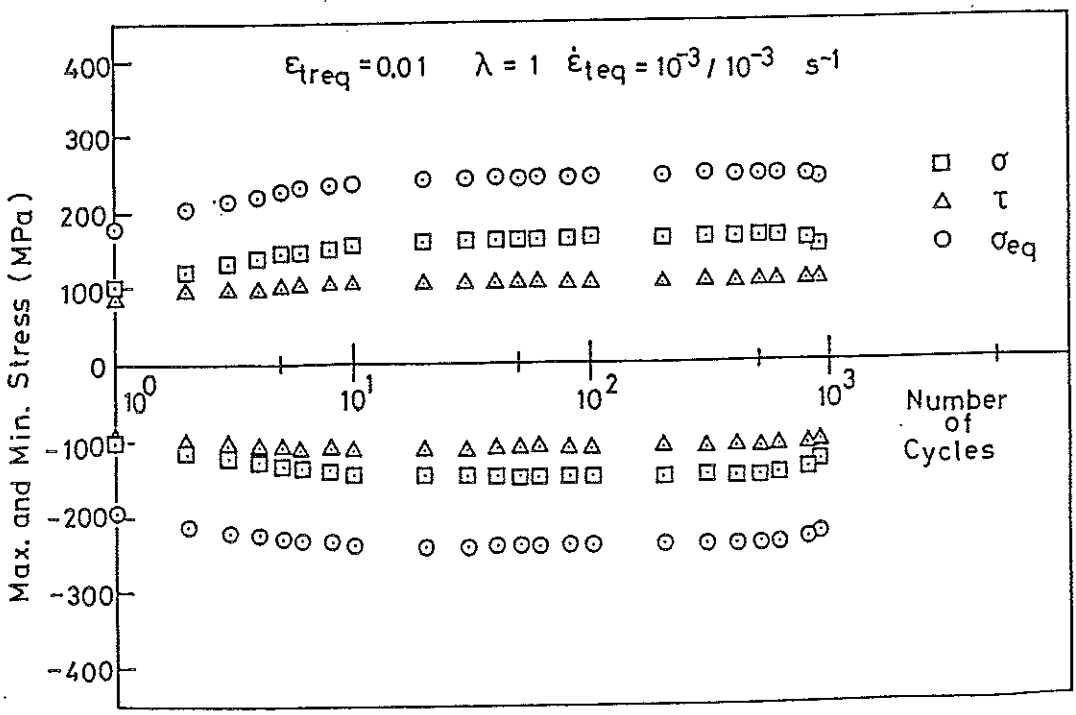

Fig. 2 Cyclic Strain Hardening Behavior under Biaxial Loading

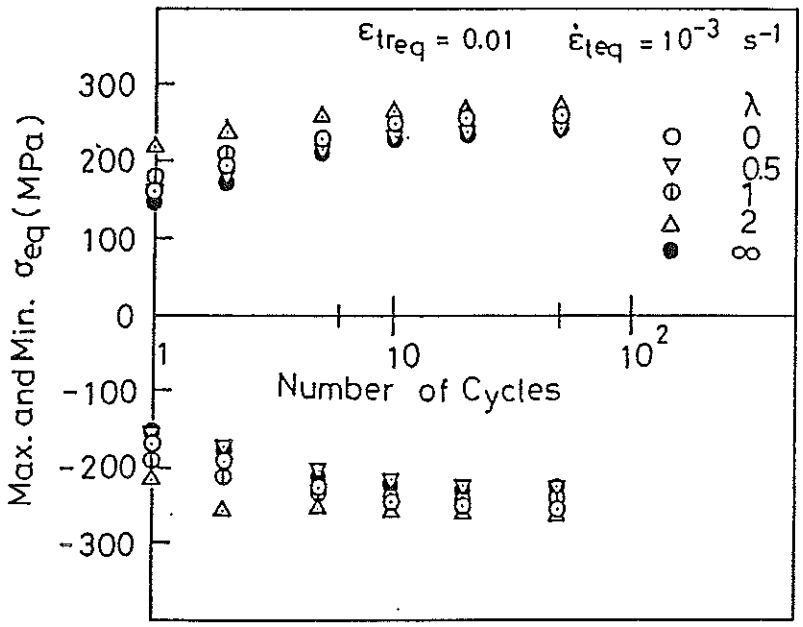

Fig. 3 Cyclic Strain Hardening Behavior under Various Values of Proportional Factor

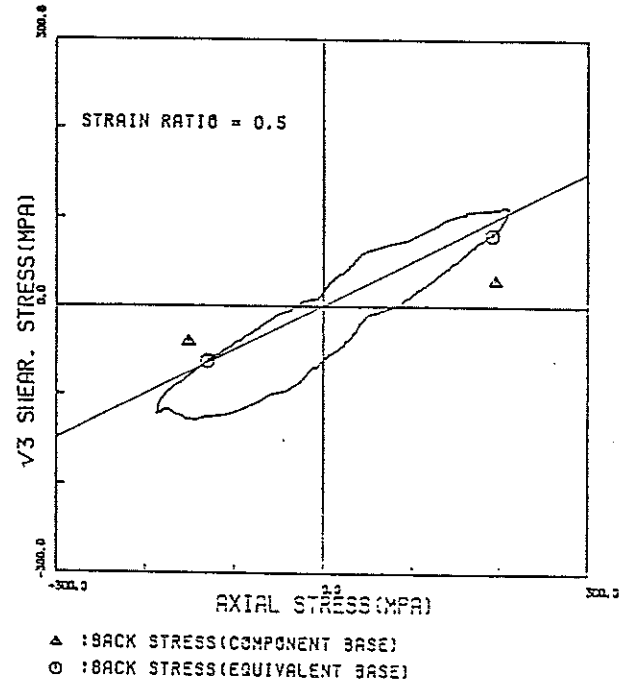

Fig. 4-a Locus of Stress Components (λ = 0.5)

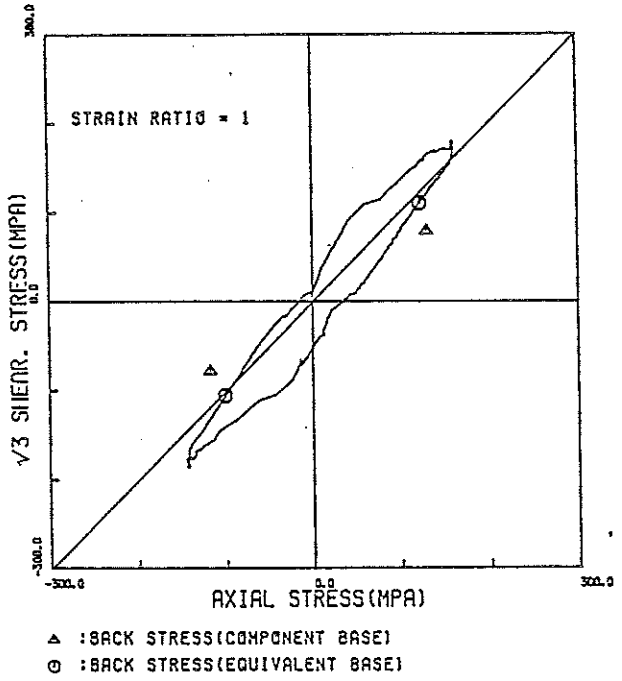

Fig. 4-b Locus of Stress Components (λ = 1)

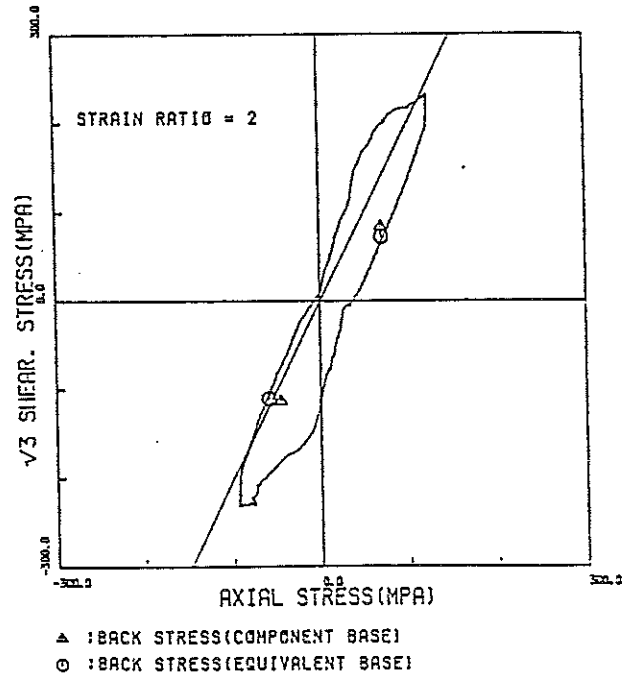

Fig. 4-c Locus of Stress Components (λ = 2)

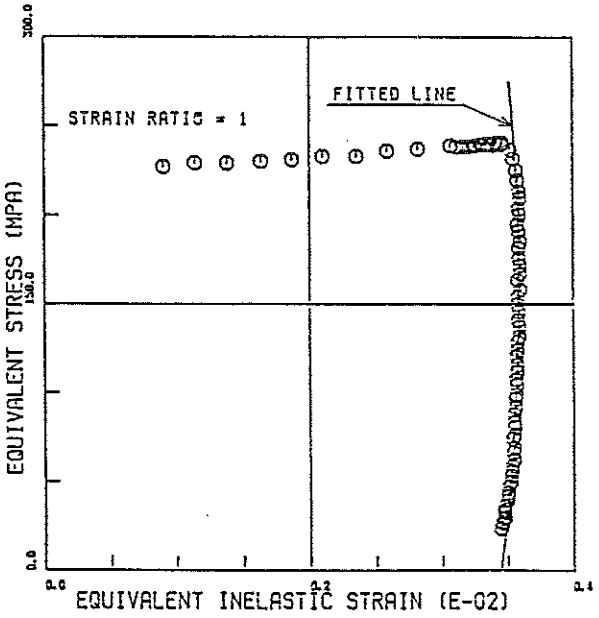

Fig. 5 Bowing-out Shape in Unloading Curve (λ = 1)

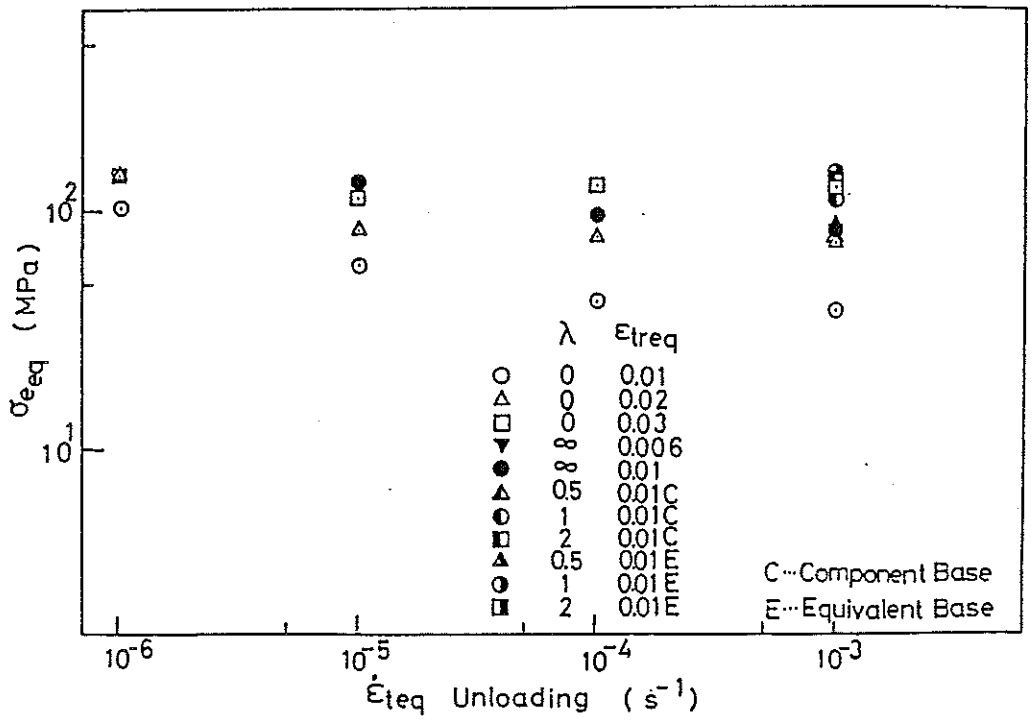

Fig. 6 Relaxation of Observed Overstress due to Unloading Strain Rate Increase

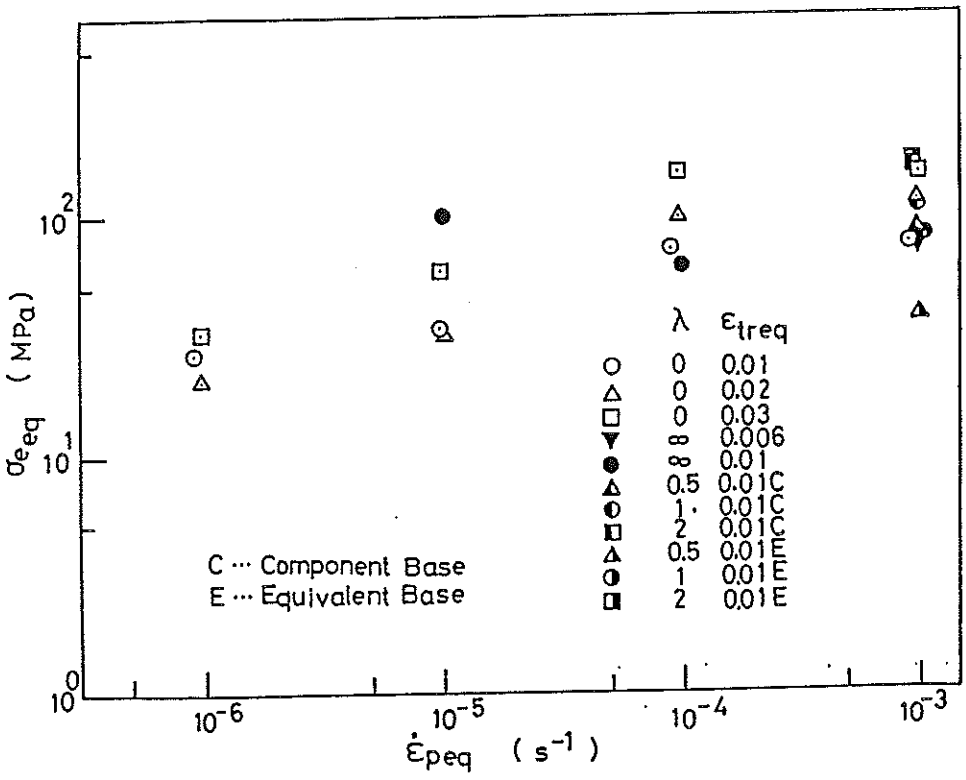

Fig. 7 Overstress versus Loading Inelastic Strain Relation

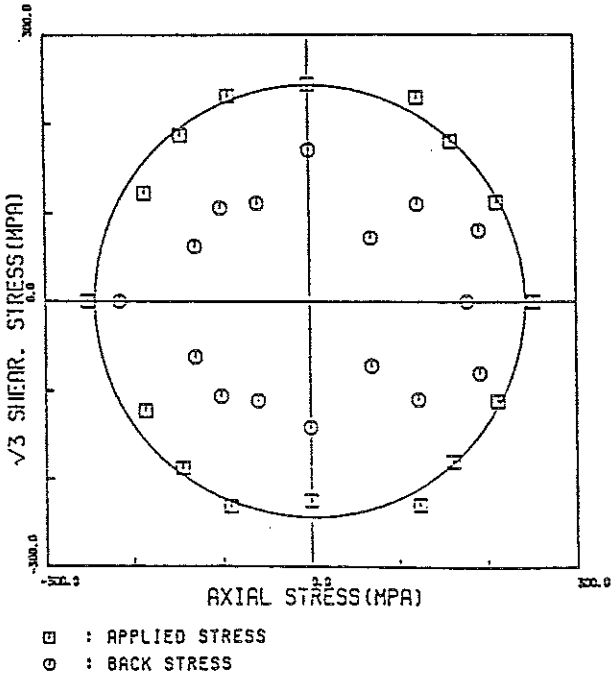

Fig. 8 Peak Stress and Back Stress Plots in Biaxial Plane
(Equivalent Stress Base)

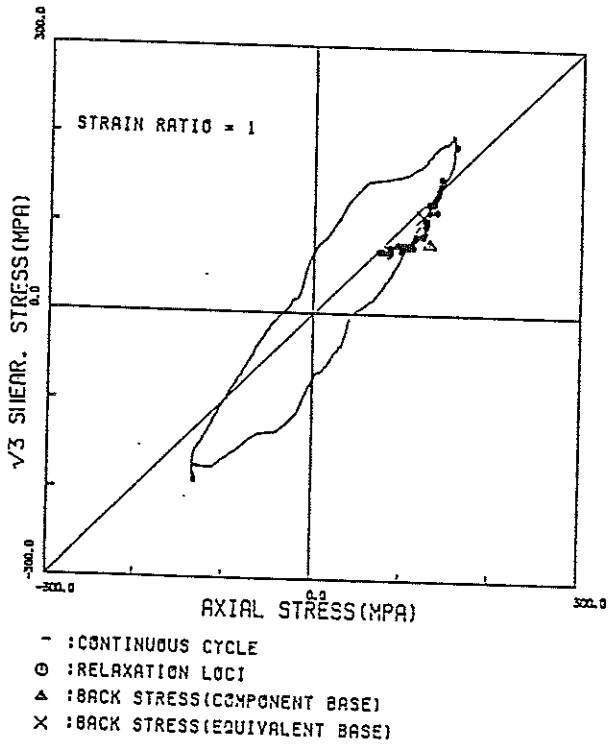

Fig. 9 Locus of Stress Components during Relaxation

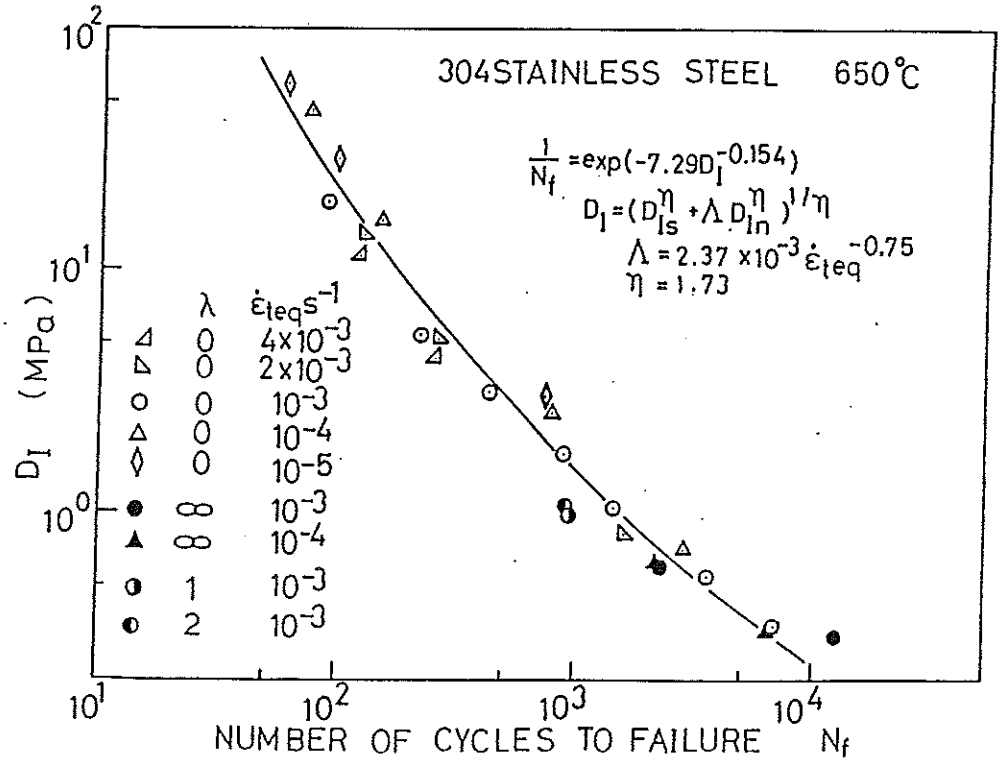

Fig. 10 Relation between Time-Independent Damage Parameter and Fatigue Life

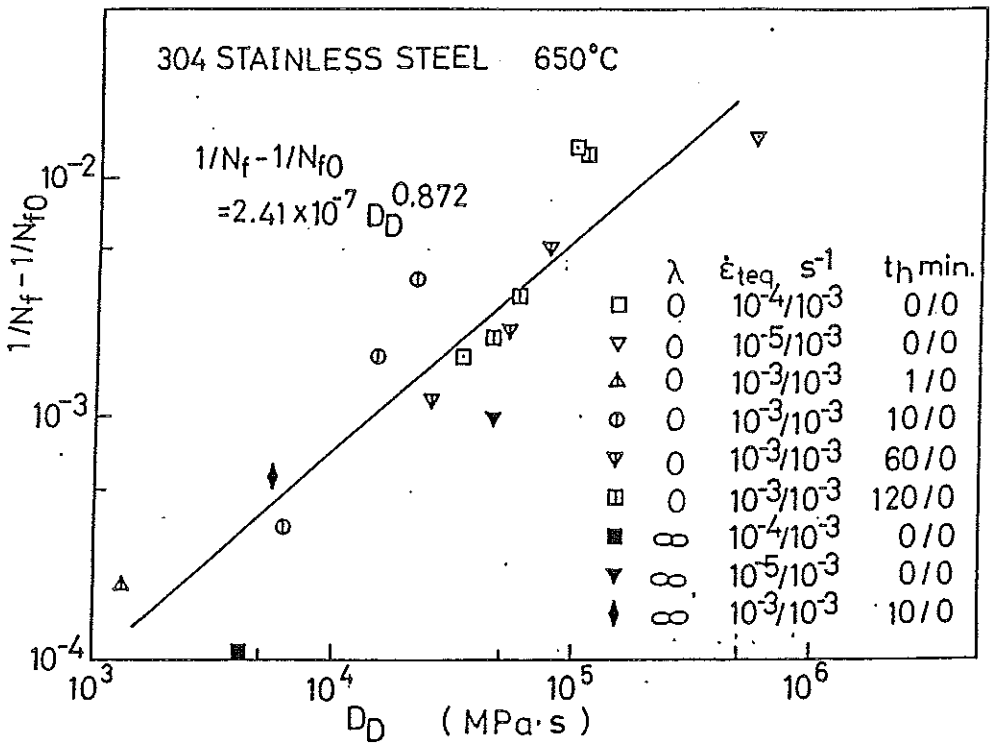

Fig. 11 Relation between Time-Dependent Damage Parameter and Fatigue Life

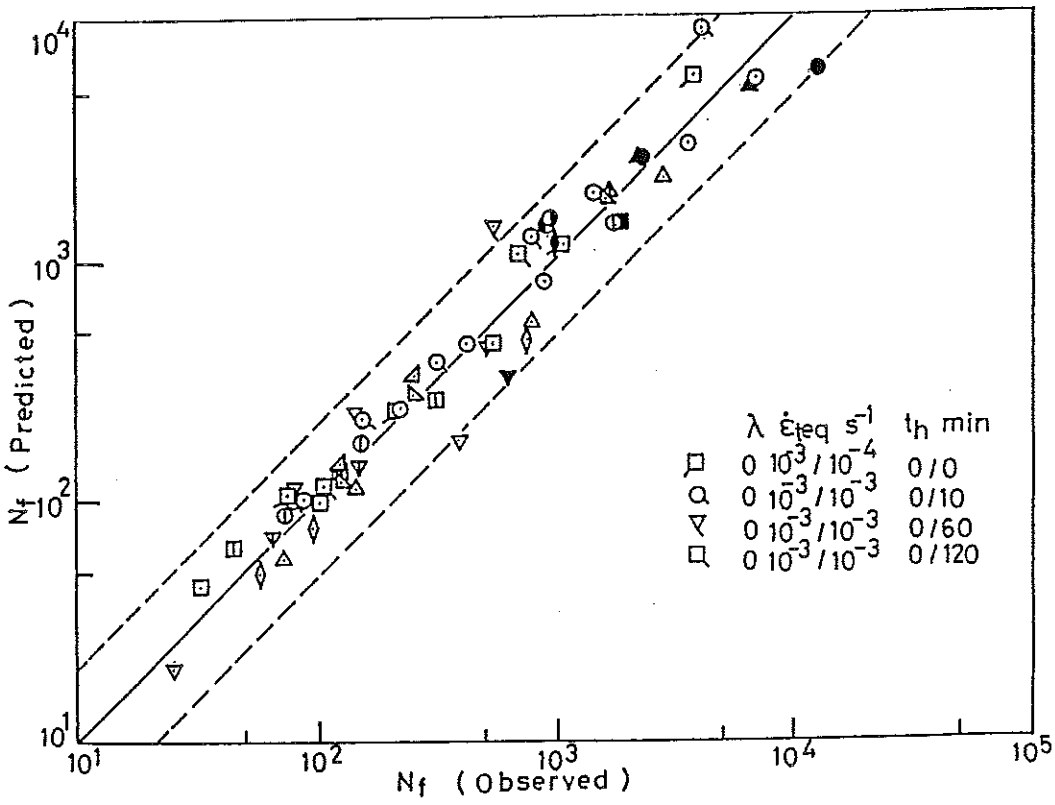

Fig. 12 Relation between Observed Life and Predicted Life